Dynamics and Control of a 5 DOF Manipulator Based on H-4 Parallel Mechanism

Kummun Chooprasird and Viboon Sangveraphunsiri
Robotics and Manufacturing Lab. Department of Mechanical Engineering
Faculty of Engineering, Chulalongkorn University,
Bangkok 10330, Thailand.
E-mail : viboon.s@eng.chula.ac.th

Abstract

This paper presents a design of a unique hybrid 5 degree-of-freedom manipulator based on a H-4 Family Parallel Mechanism with three translational movements and one rotational movement (orientation angle) together with a single axis rotating table. Forward or direct kinematics, inverse kinematics and Jacobian are derived in detail as well as the dynamic model. The dynamic model is derived from the Lagrangian formulation and is shown to be suitable in real-time feedback control. The numerical results of the analysis of kinematics, inverse kinematics and the dynamic model are compared with the result from a popular commercial software using virtual modeling data, the ADAMS solver. Friction models obtained from the experiment are used to compensate for the actual friction of the system, in the resolve acceleration control strategy. The inverse dynamics is implemented for the first four axis of the purposed configuration to perform feedback linearization. From the experimental results, the tracking performance is satisfied and can be improved by increasing the rigidity of the structure and reducing the numerical truncation error.

Keywords: H-4 Parallel Robot, Resolve acceleration, Lagrangian formulation

1. Introduction

Potential advantages of parallel mechanism over serial mechanism robots, such as structural stiffness, payload capacity, accurate precision, speed and acceleration performance, have dramatically increased the research activities related to parallel manipulators in the academic community for several years since the 6-DOF parallel mechanism for flight simulator, proposed by Gough and Stewart [18]. Although the disabilities due to the parallel configurations are the small working volume, small movement for orientation to reach a workpiece, and the large number of singularities, the benefits of these mechanisms have still been influencing development continuously in fields of robotics. Recently, many applications utilize parallel mechanisms in industries such as a high-speed laser using three RUU parallel chains (RUU: Revolute-Universal-Universal) by Delta Group, 3-DOF (RUU chains) the FlexPicker IRB 340 for high-speed picking and packing applications by ABB, 6-DOF "Hexapod" which consists of 6 UPS parallel chains (UPS: Universal-Prismatic-Spherical).

Five degrees of freedom manipulators can give the most flexibility between tool and workpiece orientation. This means that the tool can be oriented in any angle relative to a workpiece. A part with complex surfaces, such as a 3-DOF manipulator, cannot complete good enough surface cutting. Whereas, this is not the case for a 5-DOF manipulator. Besides the advantages mentioned above, the motion characteristics are also preferable, such as the errors in the arms are averaged, instead of built up as in series structures. The load is distributed to all arms, which have low inertia because the actuators are mounted on a fixed base. With benefits of these characteristics, we introduce a 5 DOF manipulator, which consisted of a H-4 parallel manipulator with addition of a single axis rotating table, to use for cutting complex surfaces. The fifth axis has to be located at a suitable location to avoid the effects of singularities and useless workspace of the H-4 robot which is mentioned in [14]. The purposed manipulator (slave arm) with the 6-DOF haptic device (master arm) developed in-house [15] can be used as tele-operation with force reflection. Force control algorithms are implemented to help an operator to gain better feeling of maneuvering the master arm during the slave arm cutting a surface as shown in Figure 1. In this paper, we concentrated only on the slave arm. The complete operation will be presented in the future.
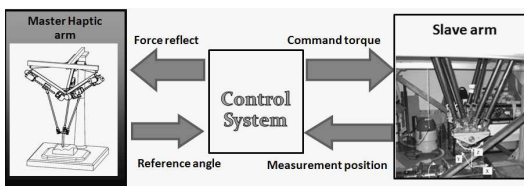

Figure 1 The tele-operation with force reflection

Multiple close-chain links make the dynamic analysis of parallel manipulators more complicated than serial manipulators.

Dynamic analysis of various types of parallel mechanisms has been studied by many researchers. Do and Yang, 1988; Guglielmetti and Longchamp, 1994; Tsai and Kohli, 1990 formulated dynamic models from the Newton-Euler method. While Lebret 1993; Miller and Clavel, 1992; Miller and Clavel, 1992; Pang and Shahingpoor, 1994, used the Lagrange Equations method. The virtual work method was studied by Codourey and Burdet, 1997; Miller, 1995; Tsai,1998; Wang and Gosselin, 1997; Zhang and Song, 1993. To obtain a dynamic model using the Newton-Euler formulation, the equations of motion of each body need to be written. This leads to a large number of equations and consumes large computation time when used in a real-time control system. Unnecessary computation of reaction forces as done in the Newton-Euler formulation are eliminated in the Lagrangian formulation. Additional coordinates along with a set of Lagrangian and some model simplification make the Lagrange formulation more efficient than the Newton-Euler formulation. This technique requires only the kinetic and potential energies of the system to be computed, and hence tends to be less prone to error than summing together the inertial, Coriolis, centrifugal, actuator, and other forces acting on the robot's links.[19] Although Lagrange's equation of the first type is suitable for modeling the dynamics of parallel manipulator, in this paper, the dynamic model of the H-4 parallel robot is derived by using the second type Lagrangian. Sangveraphunsiri has worked on the kinematics analysis for some time as shown in [9], [14], [15], and [16], and some of the work here is based on those pervious works.

The intention of this paper is to evaluate the kinematics of a 5-DOF manipulator based on the H-4 family parallel structure as in [14] together with one rotational table as shown in Figure 2. The computer simulation using the commer-

cial software (ADAMS solver), with the virtual model data of the system, is carried out to compare the results from the dynamic model derived. From the simulation results, it is shown that the complexity and this kind of configuration is suitable for complex surface machining applications with or without cutting force control. Of course, the tele-operation with force reflecting control can also be implemented with this configuration.

2. Design Consideration

The desired H-4 parallel robot must have at least 4-DOF, which will produce 3 translation motions and 1 rotary motion. In order to have large rotational movement in the y-axis, the mechanism consists of two mechanical chains connected to two separated platforms. Each chain has two degrees of freedom moving along the x-axis of the platform as shown in Figure 2. The workspace depends on the 4 parameters: the length of limb, R, the size of platform, $2c$,

the difference between the robot frame and the platform, (a-b), and the offset between two separated rails, $2d$ as shown in [14]. The 4 joint variables (l_1, l_2, l_3, and l_4) are used for specifying the location in (x, y, z) and rotation in the y-axis of the tool tip. The mobility of platform is derived in [14]. In addition to this 4-DOF, a rotary table in the x-direction is combined as a joint variable (α) to have a 5-DOF mechanism.

3. Kinematics Modeling

In this section, the relationships between the joint variables of the 5-DOF of the mechanism, $\mathbf{q} = [l_1 \ l_2 \ l_3 \ l_4 \ \alpha]$ and working or workpiece coordinate system $\mathbf{x} = [x_w \ y_w \ z_w \ I_w \ J_w \ K_w]$ have been derived as shown in Figure 1. I_w, J_w and K_w are the directional cosines of the working frame $[x_w \ y_w \ z_w]$. The geometric configuration of robot parameters are given in Figure 2.
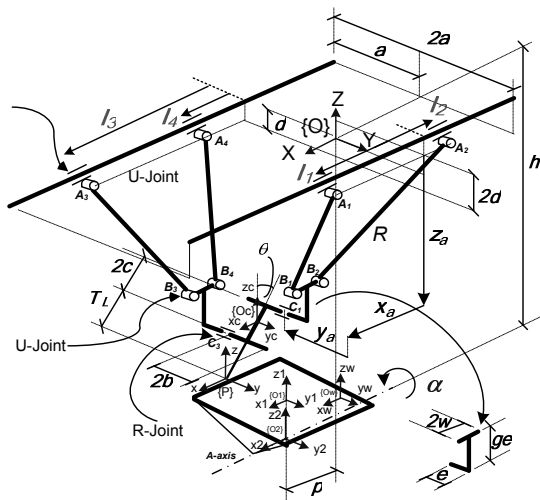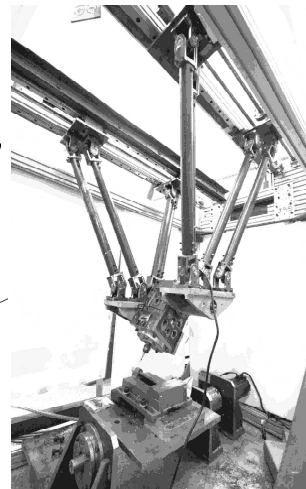

Figure 2 Manipulator joint configurations

  R Length of limb
  $2a$ Distance in Y direction between two offset rails
  $2b$ Wide size of the platform
  $2c$ Long size of the platform

  $2d$ Distance in Z direction between two offset rails
  h Distance in Z direction between reference frame and rotating table axis (A-axis)

p Distance in X direction between reference frame and frame {O2}

$2w$ Length in X direction between center (B_i) of two universal joints.

e Length in Y direction between location of both U-joints (B_i, B_{i+1}) and revolute joint (C_i)

ge Length in Z direction between location of both U-joints (B_i, B_{i+1}) and revolute joint (C_i)

T_L Length of Tool

3.1 Inverse Kinematics

Typically, working paths are defined in Cartesian space or the working coordinate system. Inverse kinematics is used for obtaining the joint commands from the specified working paths.

In Figure 2, vector $\mathbf{C_1B_1}$ and $\mathbf{C_1B_2}$ are symmetric about the $\mathbf{Z_cY_c}$-plane if $\theta = 0$ and vector $\mathbf{O_cC_1}$ and $\mathbf{O_cC_3}$ point in the opposite direction. The coordinate $[x_a, y_a, z_a]$ represents the vector position of point $\mathbf{C_1}$ with respect to origin of the link l_1 or l_2. The inverse position can be obtained as follows:

$$l_1 = x_a + w + \sqrt{R^2 - (y_a - e)^2 - (z_a - ge)^2} \quad (1)$$

$$l_2 = x_a - w - \sqrt{R^2 - (y_a - e)^2 - (z_a - ge)^2} \quad (2)$$

From Figures 3 and 4, the tool-tip coordinate frame, $\{x, y, z\}$, the center of platform coordinate frame, $\{x_c, y_c, z_c\}$, and the coordinate $\{x_a, y_a, z_a\}$ can be related as shown in equations (1a) to (1c).
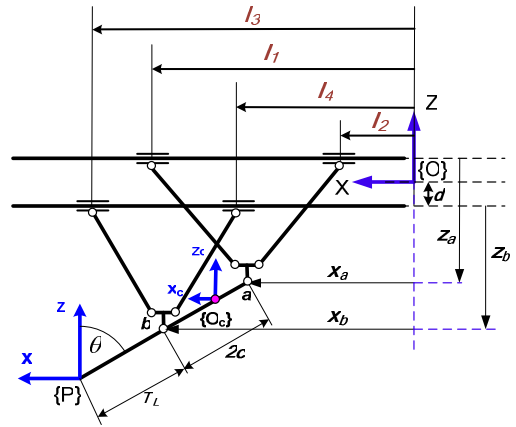

Figure 3 New variables defined as observed from the side of the manipulator

$$x_a = x - (T_L + 2c) \cdot sin(-\theta) \quad (1a)$$
$$= x_c - c \cdot sin(-\theta)$$
$$y_a = -y + a - b \quad (2b)$$
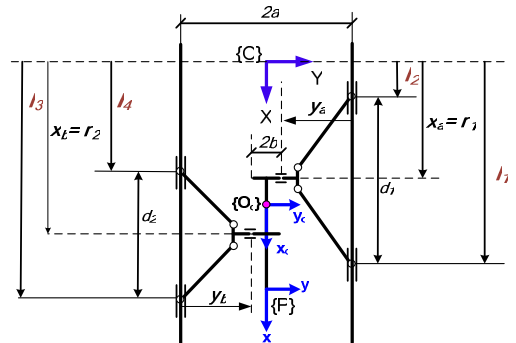$$z_a = -z - (T_L + 2c) \cdot cos(-\theta) + d \quad (1c)$$

Figure 4 New variables defined as observed from the top of the manipulator

The other actuator-end effecter positions with the variables x_b, y_b, z_b, the relationship becomes:

$$l_3 = x_b + w + \sqrt{R^2 - (y_b - e)^2 - (z_b - ge)^2} \quad (3)$$

$$l_4 = x_b - w - \sqrt{R^2 - (y_b - e)^2 - (z_b - ge)^2} \quad (4)$$

where (x_b, y_b, z_b) are the coordinates of the point $\mathbf{C_3}$ with respect to the origin of

the link l_3 or l_4. In Figures 3 and 4, the variables x_b, y_b, z_b, the tool-tip coordinate frame and the center of platform coordinate frame, can be found as:

$$x_b = x - T_L \cdot sin(-\theta) = x_c + c \cdot sin(-\theta)$$
(2a)

$$y_b = y + a - b = y_c + a - b \qquad (2b)$$

$$Zb = z - d - T_L cos(-\theta) \qquad (2c)$$

By using geometric transformation, as shown in Figure 5, the transfor-mation from the workpiece coordinate to the reference coordinate is as follows:

$$\{O_w\} \xrightarrow{\mathsf{T}} \{O_1\} \xrightarrow{\mathsf{T}} \{O_2\} \xrightarrow{\mathsf{R}} \{O_2\} \xrightarrow{\mathsf{T}} \{O\}$$

where T means translation and R means rotation.

The expressions between work-piece coordinate and the reference coor-dinate are:

$$
\begin{bmatrix} x \\ y \\ z \\ 1 \end{bmatrix} =
\begin{bmatrix}
1 & 0 & 0 & x_{Ow}^{O1} + p \\
0 & cos\alpha & -sin\alpha & y_{Ow}^{O1}cos\alpha - z_{O1}^{O2}sin\alpha \\
0 & sin\alpha & cos\alpha & y_{Ow}^{O1}sin\alpha + z_{O1}^{O2}cos\alpha - h \\
0 & 0 & 0 & 1
\end{bmatrix}
\begin{bmatrix} x_w \\ y_w \\ z_w \\ 1 \end{bmatrix}
\qquad (3a)
$$

where $x_{Ow}^{O1}, y_{Ow}^{O1}, z_{Ow}^{O1}$ mean the coordinates with the origin at O_w written in frame O_1 and z_{O1}^{O2} is the coordinate of the origin O_1 in frame O_2.
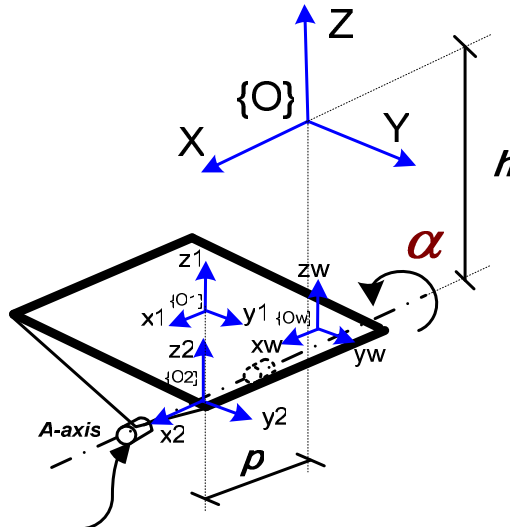

Figure 5 The Workpiece Table Reference Position and Intermediate Reference Sys-tems

The end of the tooltip {P} has to be located on the surface of the workpiece. So, from the expressions (1a) - (1c) and (3a), substitute all in the equation (1), (2) and this yields:

$$l_1 = (x_w + x_{Ow}^{O1} + p) + (T_L + 2c)sin(\theta) + w + \sqrt{\begin{array}{l} R^2 - [-(y_w + y_{Ow}^{O1})cos\alpha + \\ (z_w + z_{O1}^{O2})sin\alpha - b + a - e]^2 - \\ [-(y_w + y_{Ow}^{O1})sin\alpha - (z_w + z_{O1}^{O2})cos\alpha + \\ h - (T_L + 2c)cos(\theta) + d - ge]^2 \end{array}} \qquad (5)$$

$$l_2 = (x_w + x_{Ow}^{O1} + p) + (T_L + 2c)sin(\theta) - w - \sqrt{\begin{array}{l} R^2 - [-(y_w + y_{Ow}^{O1})cos\alpha + \\ (z_w + z_{O1}^{O2})sin\alpha - b + a - e]^2 - \\ [-(y_w + y_{Ow}^{O1})sin\alpha - (z_w + z_{O1}^{O2})cos\alpha + \\ h - (T_L + 2c)cos(\theta) + d - ge]^2 \end{array}} \qquad (6)$$

Similarly, from the expressions (2a)-(2c) and (3a), substitute all in the equation (3), (4) and this yields:

$$l_3 = (x_w + x_{Ow}^{O1} + p) + T_L sin(\theta) + w + \sqrt{\begin{array}{l} R^2 - [(y_w + y_{Ow}^{O1})cos\alpha - \\ (z_w + z_{O1}^{O2})sin\alpha - b + a - e]^2 - \\ [-(y_w + y_{Ow}^{O1})sin\alpha - (z_w + z_{O1}^{O2})cos\alpha + \\ h - T_L cos(\theta) - d - ge]^2 \end{array}} \qquad (7)$$

$$l_4 = (x_w + x_{Ow}^{O1} + p) + T_L sin(\theta) - w - \sqrt{\begin{array}{l} R^2 - [(y_w + y_{Ow}^{O1})cos\alpha - \\ (z_w + z_{O1}^{O2})sin\alpha - b + a - e]^2 - \\ [-(y_w + y_{Ow}^{O1})sin\alpha - (z_w + z_{O1}^{O2})cos\alpha + \\ h - T_L cos(\theta) - d - ge]^2 \end{array}} \qquad (8)$$

For the tooltip orientation, it has to be coincident with the direction-cosine of the position on the workpiece surface as shown in Figure 6.
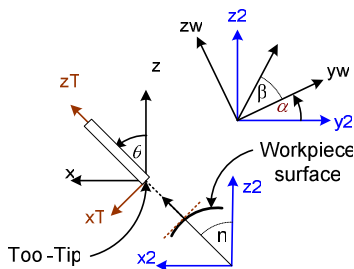

Figure 6 Tooltip orientation and workpiece direction cosine

The unit vector of the normal plane at the cutting location of a workpiece surface can be written as $I_w i_w + J_w i_w + K_w k_w$, where I_w, J_w, K_w are the direction cosines. So, the orientation can be obtained as follows:

$$\beta = \arctan\left[\frac{K_w}{J_w}\right] \qquad (4a)$$

$$I_2 = I_w \qquad (4b)$$

$$J_2 = \left(\sqrt{J_w^2 + K_w^2}\right)cos(\alpha + \beta) \qquad (4c)$$

$$K_2 = \left(\sqrt{J_w^2 + K_w^2}\right)sin(\alpha + \beta) \qquad (4d)$$

From the above equations, this yields:

$$\alpha = \pm 90° - \arctan\left[\frac{K_w}{J_w}\right]$$

where $-90° \le \alpha \le 90°$ $\qquad (9)$

$$\theta = \arctan\left[\frac{I_w}{\sqrt{J_w^2 + K_w^2}}\right]$$

where $-90° \le \theta \le 90°$ $\qquad (10)$

3.2 Forward or Direct Kinematics

In this section, the tooltip location and orientation are found from a given set of joint variables. The robot joint variables l_1, l_2, l_3, l_4 and α, shown in Figure 4, with new variables are defined as:

$$r_1 = \frac{l_1 + l_2}{2}, r_2 = \frac{l_3 + l_4}{2}$$

$$d_1 = l_1 - l_2, d_2 = l_3 - l_4 \qquad (11)$$

By observation of Figure 3, the rotation angle (θ) of the platform can readily be determined as:

$$cos\theta = \frac{\sqrt{4c^2 - (r_2 - r_1)^2}}{2c} \qquad (12)$$

From equation (1a) and Figure 3-4, the movement in the x direction is obtained as:

$$x = \left[\frac{r_1 + r_2}{2}\right] - (c + T_L)sin\theta \qquad (13)$$

By observation of Figure 4, the expressions using the new variables are:

$$(l_2 - x_a)^2 = (l_1 - x_a)^2 = \frac{d_1^2}{4} \qquad (14)$$

$$(l_4 - x_b)^2 = (l_3 - x_b)^2 = \frac{d_1^2}{4} \qquad (15)$$

To find motion in y and z directions, manipulate (1) to (4) together with (14), (15), yielding y in terms of z_c in two equations as:

$$y = y_c = \frac{d_1^2 - d_2^2 - 4w(d_1 - d_2) - 16(d - c\cos\theta)(z_c + ge)}{16(a - b - e)} \qquad (16)$$

$$z_c^2\left[\frac{16^2(d - c\cos\theta)^2}{128(a - b - e)^2} + 2\right] + z_c\left[4ge\frac{32(d - c\cos\theta)(d_1^2 - d_2^2 - 4w(d_1 - d_2)) - 512ge(d - c\cos\theta)^2}{128(a - b - e)^2}\right] +$$

$$\left[\frac{16^2(d - c\cos\theta)^2 ge^2(d - c\cos\theta)(d_1^2 - d_2^2 - 4w(d_1 - d_2))}{128(a - b - e)^2} + \frac{(d_1^2 - d_2^2 - 4w(d_1 - d_2))^2}{128(a - b - e)^2} + \right.$$

$$\left. 2w^2 - w(d_1 + d_2) + 2ge^2 + \frac{(d_1^2 + d_2^2)}{4} - 2R^2 + 2(b - a)^2 - 4e(a - b) + 2e^2 + 2(c\cos\theta - d)\right]^2 = 0$$

$$(17)$$

From equation (17), the 2nd degree polynomial formula can be solved from:

$$z_c = \frac{-B \pm \sqrt{B^2 - 4AC}}{2A} \qquad (18)$$

where

$$A = \left[\frac{16^2 (d - c\cos\theta)^2}{128(a - b - e)^2} + 2 \right] \qquad (18a)$$

$$B = \left[4ge + \frac{512 ge(d - c\cos\theta)^2}{128(a - b - e)^2} - \frac{32(d - c\cos\theta)(d_1^2 - d_2^2 - 4w(d_1 - d_2))}{128(a - b - e)^2} \right] \qquad (18b)$$

$$C = \left| \begin{array}{l} \dfrac{6^2 (d - c\cos\theta)^2 ge^2}{128(a - b - e)^2} - \dfrac{32(d - c\cos\theta)(d_1^2 - d_2^2 - 4w(d_1 - d_2))}{128(a - b - e)^2} + \\[3mm] \dfrac{(d_1^2 - d_2^2 - 4w(d_1 - d_2))^2}{128(a - b - e)^2} + \dfrac{(d_1^2 + d_2^2)}{4} + 2w^2 - w(d_1 + d_2) + 2ge^2 + \\[3mm] 2e^2 - 2R^2 + 2(b - a)^2 - 4e(a - b) + 2(c\cos\theta - d)^2 \end{array} \right| \qquad (18c)$$

Due to the configuration of robot, the solution in the z_c direction is always negative and z can be found as:

$$z = z_c - (c + T_L)\cos\theta \qquad (19)$$

The reference coordinates relate to the workpiece coordinates by transforma-tion as:

$$\{O\} \xrightarrow{T} \{O_2\} \xrightarrow{R} \{O_2\} \xrightarrow{T} \{O_1\} \xrightarrow{T} \{O_w\}$$

The tool-tip contact location on the workpiece surface can be expressed by:

$$\begin{bmatrix} x_w \\ y_w \\ z_w \\ 1 \end{bmatrix} = \begin{bmatrix} 1 & 0 & 0 & x_{O1}^{Ow} - p \\ 0 & \cos\alpha & \sin\alpha & y_{O1}^{Ow} + h\sin\alpha \\ 0 & -\sin\alpha & \cos\alpha & z_{O21}^{O1} + h\cos\alpha \\ 0 & 0 & 0 & 1 \end{bmatrix} \begin{bmatrix} x \\ y \\ z \\ 1 \end{bmatrix} \qquad (6a)$$

By manipulating equations (11), (13), (16), (18), (19) and substituting all in (6a), this yield:

$$x_w = \left[\frac{l_1 + l_2 + l_3 + l_4}{4} \right] - (c + T_L)\sin\theta - p + x_{O1}^{Ow} \qquad (7a)$$

$$y_w = \left[\frac{-B \pm \sqrt{B^2 - 4AC}}{2A} - (c + T_L)\cos\theta \right]\sin\alpha + h\sin\alpha + y_{O1}^{Ow} +$$

$$\left[\frac{d_1^2 - d_2^2 - 4w(d_1 - d_2) - 16(d - c\cos\theta)\left[\dfrac{-B \pm \sqrt{B^2 - 4AC}}{2A} + ge \right]}{16(a - b - e)} \right]\cos\alpha \qquad (7b)$$

$$z_w = \left[\frac{-B \pm \sqrt{B^2 - 4AC}}{2A} - (c + T_L)\cos\theta \right]\cos\alpha + h\cos\alpha + z_{O2}^{O1} -$$

$$\left[\frac{d_1^2 - d_2^2 - 4w(d_1 - d_2) - 16(d - c\cos\theta)\left[\dfrac{-B \pm \sqrt{B^2 - 4AC}}{2A} + ge \right]}{16(a - b - e)} \right]\sin\alpha \qquad (7c)$$

The direction cosines of the work-piece cutting location, or tool-tip contact point, from angle θ and α can be found as:

$$I_w = \pm \frac{1}{\sqrt{1 + \dfrac{1}{\tan^2\theta}}} \qquad (8a)$$

where $sign(I_w) = sign(\theta)$

$$J_w = \pm \frac{1}{(\sqrt{1 + \tan^2\theta})(\sqrt{1 + \tan^2(90 - \alpha)})} \qquad (8b)$$

where $sign(J_w) = sign(\alpha)$

$$K_w = \frac{\tan(90 - \alpha)}{(\sqrt{1 + \tan^2\theta})(\sqrt{1 + \tan^2(90 - \alpha)})} \qquad (8c)$$

where $sign(K_w) = +$

3.3 Manipulator Jacobian Matrix

In order to obtain the velocity relationship between the joint variables and the working coordinate, the position relationship are differentiated instead.

Knowing the velocity vector on the platform relative to the rotating table directly, this can be obtained by the relationship of the velocity of the tool attached relative to the moving table which is represented by $X_T^{TP} = [x_w \, y_w \, z_w \, \theta \alpha]^T$ and the actuator input denoted by **q** as follows:

From Figure 2, the tool-tip velocity of platform (V_P) can be written as:

$$V_{Bi} = V_{Bi+1} = V_{Ci} = V_P + \theta j \times PC_i \qquad (20)$$

Then, the velocity at point B related to that of point A is:

$$A_i B_i \bullet V_{Ai} = A_i B_i \bullet V_{Bi} \qquad (21)$$

According to [2], the Jacobian matrix of the machine can be written in the form of:

$$A\dot{q} = B\dot{x} \qquad (22)$$

$$\dot{q} = J\dot{x} \text{ where } J = A^{-1}B \qquad (23)$$

So,

$$A_i B_i \bullet V_{Ai} = A_i B_i \bullet V_{P/w} - A_i B_i \bullet \alpha \left(\sqrt{y_w^2 + (z_w + z_{O1}^{O2})^2} \right) i + (PC_i \times A_i B_i) \bullet \dot{\theta} \, j \tag{24}$$

$$A = \begin{vmatrix} A_i B_i \bullet i & 0 & 0 & 0 & 0 \\ 0 & A_i B_i \bullet i & 0 & 0 & 0 \\ 0 & 0 & A_i B_i \bullet i & 0 & 0 \\ 0 & 0 & 0 & A_i B_i \bullet i & 0 \\ 0 & 0 & 0 & 0 & 1 \end{vmatrix} \tag{24a}$$

$$q = \begin{bmatrix} l_1 & l_2 & l_3 & l_4 & \dot{\alpha} \end{bmatrix}^T \tag{24b}$$

$$B = \begin{vmatrix} A_1 B_1 \bullet u_{P/w}(PC_1 \times A_1 B_1) \bullet j - A_1 B_1 \bullet (\sqrt{y_w^2 + (z_w + z_{O1}^{O2})^2}\,)i \\ A_2 B_2 \bullet u_{P/w}(PC_2 \times A_2 B_2) \bullet j - A_2 B_2 \bullet (\sqrt{y_w^2 + (z_w + z_{O1}^{O2})^2}\,)i \\ A_3 B_3 \bullet u_{P/w}(PC_3 \times A_3 B_3) \bullet j - A_3 B_3 \bullet (\sqrt{y_w^2 + (z_w + z_{O1}^{O2})^2}\,)i \\ A_4 B_4 \bullet u_{P/w}(PC_4 \times A_4 B_4) \bullet j - A_4 B_4 \bullet (\sqrt{y_w^2 + (z_w + z_{O1}^{O2})^2}\,)i \\ 0 \qquad\qquad 0 \qquad\qquad\qquad i \end{vmatrix} \tag{24c}$$

$$\dot{x}_T^{TP} = \begin{bmatrix} \dot{x}_w & \dot{y}_w & \dot{z}_w & \dot{\theta} & \dot{\alpha} \end{bmatrix}^T \tag{24d}$$

From equation $\dot{q} = J\dot{x}$, analytical Jacobian (J) can obtained by taking deri- vatives on the inverse kinematics equations (5) to (8) as follow:

$$j = \begin{vmatrix} 1 & -A_x^{-\frac{1}{2}}(B_x\cos\alpha + C_x\sin\alpha) & A_x^{-\frac{1}{2}}(B_x\cos\alpha - C_x\sin\alpha) & (T_L+2c)\left[\cos\theta + A_x^{-\frac{1}{2}}C_x\sin\theta\right] & A_x^{-\frac{1}{2}}\left[\begin{matrix}B_x\left[(y_w+y_{Ow}^{O1})\sin\alpha + (z_w+z_{O1}^{O2})\cos\alpha\right]+ \\ C_x\left[(z_w+z_{O1}^{O2})\sin\alpha - (y_w+y_{Ow}^{O1})\cos\alpha\right]\end{matrix}\right] \\ 1 & A_x^{-\frac{1}{2}}(B_x\cos\alpha + C_x\sin\alpha) & A_x^{-\frac{1}{2}}(B_x\sin\alpha - C_x\cos\alpha) & (T_L+2c)\left[\cos\theta - A_x^{-\frac{1}{2}}C_x\sin\theta\right] & -A_x^{-\frac{1}{2}}\left[\begin{matrix}B_x\left[(y_w+y_{Ow}^{O1})\sin\alpha + (z_w+z_{O1}^{O2})\cos\alpha\right]+ \\ C_x\left[(z_w+z_{O1}^{O2})\sin\alpha - (y_w+y_{Ow}^{O1})\cos\alpha\right]\end{matrix}\right] \\ 1 & -A_y^{-\frac{1}{2}}(B_y\cos\alpha + C_y\sin\alpha) & A_y^{-\frac{1}{2}}(B_y\sin\alpha - C_y\cos\alpha) & T_L\left[\cos\theta + A_y^{-\frac{1}{2}}C_y\sin\theta\right] & A_y^{-\frac{1}{2}}\left[\begin{matrix}B_y\left[(y_w+y_{Ow}^{O1})\sin\alpha + (z_w+z_{O1}^{O2})\cos\alpha\right]+ \\ C_y\left[(z_w+z_{O1}^{O2})\sin\alpha - (y_w+y_{Ow}^{O1})\cos\alpha\right]\end{matrix}\right] \\ 1 & A_y^{-\frac{1}{2}}(B_y\cos\alpha + C_y\sin\alpha) & -A_y^{-\frac{1}{2}}(B_y\sin\alpha - C_y\cos\alpha) & T_L\left[\cos\theta - A_y^{-\frac{1}{2}}C_y\sin\theta\right] & -A_x^{-\frac{1}{2}}\left[\begin{matrix}B_y\left[(y_w+y_{Ow}^{O1})\sin\alpha + (z_w+z_{O1}^{O2})\cos\alpha\right]+ \\ C_y\left[(z_w+z_{O1}^{O2})\sin\alpha - (y_w+y_{Ow}^{O1})\cos\alpha\right]\end{matrix}\right] \\ 0 & 0 & 0 & 0 & 1 \end{vmatrix} \tag{25}$$

where

$$A_x = R^2 - B_x^2 - C_x^2 \tag{25a}$$

$$B_x = (y_w + y_{Ow}^{O1})\cos\alpha - (z_w + z_{O1}^{O2})\sin\alpha + b - a + e \tag{25b}$$

$$C_x = (y_w + y_{Ow}^{O1})\sin\alpha + (z_w + z_{O1}^{O2})\cos\alpha - h + (T_L + 2C)\cos(\theta) - d + ge \tag{25c}$$

and

$$A_y = R^2 - B_y^2 - C_y^2 \tag{25d}$$

$$B_y = (y_w + y_{Ow}^{O1})\cos\alpha - (z_w + z_{O1}^{O2})\sin\alpha - b + a - e \tag{25e}$$

$$C_y = (y_w + y_{Ow}^{O1})\sin\alpha + (z_w + z_{O1}^{O2})\cos\alpha - h + (T_L\cos(\theta) + d + ge \tag{25f}$$

4. Analytical Dynamics Model

In this section, the conservative Lagrange's equation is used to obtain the dynamic model of the closed-chain H-4 type from the forward kinematics derived earlier. The Lagrangian is defined as the difference between the kinetic energy and the potential energy of a mechanical system:

$$L = K.E. - P.E. \qquad (26)$$

The kinetic energy depends on both location and velocity of the manipulator linkages, whereas the potential energy depends only on the location of the links. For a conservative system, the well-known generalized Lagrange's equation of coordinates q_i, with generalized force Q_i, can be written as:

$$\frac{d}{dt}\left[\frac{\partial L}{\partial \dot{q}_i}\right] - \frac{\partial L}{\partial q_i} \qquad i=1,2,n... \quad (27)$$

Replace expression (26) in (27):

$$\frac{d}{dt}\frac{\partial(K.E.)}{\partial \dot{q}_i} - \frac{\partial(K.E.)}{\partial q_i} + \frac{\partial(P.E.)}{\partial q_i} = Q_i \quad (28)$$

According to Figure 7, the robot manipulator consists of 5 components which can be detailed as following:

- Platform *(p or MH)* 1 part.
- Connecting Head *(CH)* 2 parts.
- Arm or link *(Am)* 8 parts.
- Linear joint *(LJ)* 4 parts.
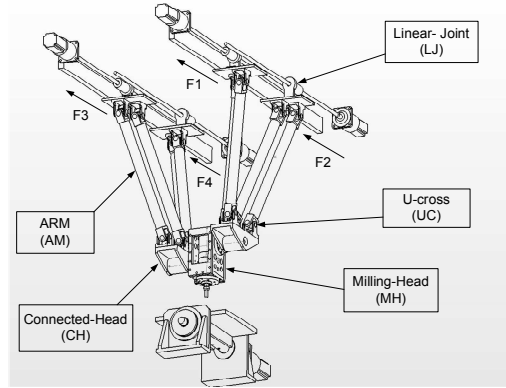- Universal joint *(UC)* 16 parts.

Figure 7 Robot Components in Virtual prototype of a 5 DOF H-4 type.

By considering all of the robot components, the Lagrange equation based on the coordinates of the linear joint l_i of 4-DOF can be derived as follows:

$$\frac{d}{dt}\frac{\partial(K.E_P)}{\partial \dot{l}_i} - \frac{\partial(K.E_p)}{\partial l_i} + \frac{\partial(P.E_P)}{\partial l_i} = F_{pi} \quad (29a)$$

$$\frac{d}{dt}\frac{\partial(\sum_{j=1}^{2} K.E_{CHj})}{\partial \dot{l}_i} - \frac{\partial(\sum_{j=1}^{2} K.E_{CHj})}{\partial l_i} + \frac{\partial(\sum_{j=1}^{2} P.E_{CHj})}{\partial l_i} = \sum_{j=1}^{2} F_{CHji}$$
$$(29b)$$

$$\frac{d}{dt}\frac{\partial(\sum_{j=1}^{8} K.E_{Amj})}{\partial \dot{l}_i} - \frac{\partial(\sum_{j=1}^{8} K.E_{Amj})}{\partial l_i} + \frac{\partial(\sum_{j=1}^{8} P.E_{Amj})}{\partial l_i} = \sum_{j=1}^{8} F_{Amji}$$
$$(29c)$$

$$\frac{d}{dt}\frac{\partial(\sum_{j=1}^{4} K.E_{LJj})}{\partial \dot{l}_i} = \sum_{j=1}^{4} m_{LJj}l_i = \sum_{j=1}^{4} F_{LJji} \qquad (29d)$$

$$\frac{d}{dt}\frac{\partial(\sum_{j=1}^{16} K.E_{UCj})}{\partial \dot{l}_i} - \frac{\partial(\sum_{j=1}^{16} K.E_{UCj})}{\partial l_i} + \frac{\partial(\sum_{j=1}^{16} P.E_{UCj})}{\partial l_i} = \sum_{j=1}^{16} F_{UCji}$$
$$(29e)$$

where $i=1,2,3,4$

By Summing equations (29a)-(29e), the equation of motion of the system is:

$$\frac{d}{dt}\frac{\partial(K.E.)}{\partial \dot{l}_i} - \frac{\partial(K.E.)}{\partial l_i} + \frac{\partial(P.E.)}{\partial l_i} = F_i \quad (29)$$

$$i=1,2,3,4$$

For the first component of the manipulator, the kinetic energy and the potential energy of platform in equation (29a) can be found as:

$$K.E._p = \frac{1}{2} m_{MH} \left(\dot{x}_{MHcm}^2 + \dot{y}_{MHcm}^2 + \dot{Z}_{MHcm}^2 \right) + \frac{1}{2} \bar{I}_{MHy} \dot{\theta}^2$$ (30)

$$P.E._p = m_{MH} g. z_{MHcm}$$ (31)

From equation (30)-(31), the location variables and their derivatives of the platform component can be found and rearranged in the form of joint variables. This yields:

$$x_{MHcm} = D_x (l_1 + l_2) + D_y (l_3 + l_4)$$ (32)

$$\dot{x}_{MHcm} = D_x (\dot{l}_1 + \dot{l}_2) + D_y (\dot{l}_3 + \dot{l}_4)$$ (33)

$$\ddot{x}_{MHcm} = D_x (\ddot{l}_1 + \ddot{l}_2) + D_y (\ddot{l}_3 + \ddot{l}_4)$$ (34)

where coefficient $D_x = \left(\frac{1}{4} - \frac{Ec}{4c} \right)$,

$D_y = \left(\frac{1}{4} + \frac{Ec}{4c} \right)$ and Ec is eccentric distance due to center of mass of platform as shown in Figure 8.
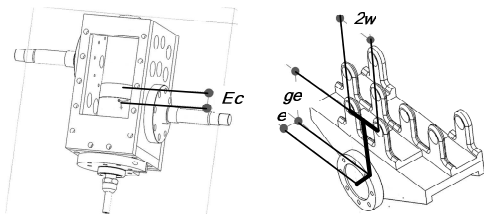
Figure 8 Platform and Connecting head Component

The coefficient A, B, C in equation (18a)-(18c) can be rearranged in terms of joint variables $l_1 \; l_2 \; l_3 \; l_4$ together with the parameters of connecting head component as shown in Figure 8: $ge = 104$, $e = 23.75$, $w = 35$, the center of mass of platform in Z and Y direction can be obtained from equation (18) as:

$$z_{MHcm} = z_c - Ec \sqrt{1 - \left[\frac{l_1 + l_2 - l_3 - l_4}{4c} \right]^2}$$ (36)

$$y_{MHcm} = \frac{(l_1 - l_2)^2 - (l_3 - l_4)^2 - 140(l_1 - l_2 - l_3 + l_4)}{16(a - b - 23.75)} - \frac{16 \left(d - c \sqrt{1 - \left(\frac{l_1 + l_2 - l_3 - l_4}{4c} \right)^2} \right)(z_c + 104)}{16(a - b - 23.75)}$$ (37)

The first time derivative of the position in Z and Y direction of the platform can be found by the derivative of equations (18), (36), (37) and (12) as:

$$\dot{z}_c = \frac{-\dot{B}}{2A} - \frac{-B\dot{B}}{2A\sqrt{B^2 - 4AC}} + \frac{\dot{C}}{\sqrt{B^2 - 4AC}} + \frac{\dot{A}C}{A\sqrt{B^2 - 4AC}} + \frac{\dot{A}B}{2A^2} + \frac{\dot{A}}{2A^2} \sqrt{B^2 - 4AC}$$ (38)

$$\dot{z}_{MHcm} = \dot{Z}_c + Ec \frac{(\dot{l}_1 + \dot{l}_2 - \dot{l}_3 - \dot{l}_4)(l_1 + l_2 - l_3 - l_4)}{16c^2 \sqrt{1 - (\frac{l_1 + l_2 - l_3 - l_4}{4c})^2}}$$ (39)

$$\dot{y}_{MHcm} = \frac{(l_1 - l_2)(\dot{l}_1 - \dot{l}_2) - (l_3 - l_4)(\dot{l}_3 - \dot{l}_4) - 70(\dot{l}_1 - \dot{l}_2 - \dot{l}_3 + \dot{l}_4)}{8(a - b - 23.75)}$$
$$- \frac{\left[d - c \sqrt{1 - (\frac{l_1 + l_2 - l_3 - l_4}{4c})^2} \right] \dot{z}_c}{(a - b - 23.75)} - \frac{(z_c + 104)(\dot{l}_1 + \dot{l}_2 - \dot{l}_3 - \dot{l}_4)(l_1 + l_2 - l_3 - l_4)}{16c(a - b - 23.75)\sqrt{1 - (\frac{l_1 + l_2 - l_3 - l_4}{4c})^2}}$$ (40)

$$\dot{\theta} = \left[\frac{\dot{l}_1 + \dot{l}_2 - \dot{l}_3 - \dot{l}_4}{4c \sqrt{1 - (\frac{l_1 + l_2}{4c} - \frac{l_3 + l_4}{4c})^2}} \right]$$ (41)

where

$$\sin(\theta) = \frac{(l_1 + l_2 - l_3 - l_4)}{4c},$$ (41a)

$$\cos(\theta) = \sqrt{1 - (\frac{l_1 + l_2 - l_3 - l_4}{4c})^2}$$ (41b)

And the second time derivative of the position in Z and Y direction of the

platform can be found by the derivative of equations (38), (39), (40) and (41) as:

$$\ddot{z}_c = \frac{\dot{B}\dot{A} - A\ddot{B}}{2A^2} + \frac{\ddot{C}\sqrt{B^2 - 4AC} - \dot{C}\left[B\dot{B} - 2(A\dot{C} + C\dot{A})\right]\sqrt{B^2 - 4AC}}{B^2 - 4AC} - \frac{A\sqrt{B^2 - 4AC}\left[B\ddot{B} + \dot{B}^2\right] - B\dot{B}\left[\dot{A}\sqrt{B^2 - 4AC} + A(B^2 - 4AC)^{\frac{1}{2}}\{B\dot{B} - 2(A\dot{C} + C\dot{A})\}\right]}{2A^2(B^2 - 4AC)}$$

$$+ \frac{A\left[\dot{A}\dot{B} + B\ddot{A}\right] - 2\dot{A}^2 B}{2A^3} + \frac{A\sqrt{B^2 - 4AC}\left[\dot{A}\dot{C} + C\ddot{A}\right] - \dot{A}C\left[\dot{A}\sqrt{B^2 - 4AC} + A(B^2 - 4AC)^{\frac{1}{2}}\{B\dot{B} - 2(A\dot{C} + C\dot{A})\}\right]}{} +$$

$$A\left[\ddot{A}\sqrt{B^2 - 4AC} + \dot{A}(B^2 - 4AC)^{\frac{1}{2}}\{B\dot{B} - 2(A\dot{C} + C\dot{A})\}\right] - 2\dot{A}^2\sqrt{B^2 - 4AC} \tag{42}$$

$$\ddot{z}_{MHcm} = \ddot{z}_c + Ec\frac{(l_1 + l_2 - l_3 - l_4)^2}{16c^2\sqrt{1 - (\frac{l_1 + l_2 - l_3 - l_4}{4c})^2}} + Ec\frac{(\ddot{l}_1 + \ddot{l}_2 - \ddot{l}_3 - \ddot{l}_4)}{\sqrt{16c^2 - (l_3 + l_4 - l_1 - l_2)^2}} - Ec\frac{(l_3 + l_4 - l_1 - l_2)(\ddot{l}_1 + \ddot{l}_2 - \ddot{l}_3 - \ddot{l}_4)^2}{\left[16c^2 - (l_3 + l_4 - l_1 - l_2)^2\right]^{\frac{3}{2}}} \tag{43}$$

$$\ddot{y}_{MHcm} = \frac{(l_1 - l_2)(\ddot{l}_1 - \ddot{l}_2) + (\dot{l}_1 - \dot{l}_2)^2 - (l_3 - l_4)(\ddot{l}_3 - \ddot{l}_4) - (\dot{l}_3 - \dot{l}_4)^2 - 70(\ddot{l}_1 - \ddot{l}_2 - \ddot{l}_3 - \ddot{l}_4)}{8(a - b - 23.75)} - \left[\frac{d - c\sqrt{1 - (\frac{l_1 + l_2 - l_3 - l_4}{4c})^2}}{a - b - 23.75}\right]$$

$$\ddot{z}_c - \left[\frac{(\dot{l}_1 + \dot{l}_2 - \dot{l}_3 - \dot{l}_4)(l_1 + l_2 - l_3 - l_4)}{8c(a - b - 23.75)\sqrt{1 - \frac{l_1 + l_2 - l_3 - l_4}{4c}^2}}\right]\dot{z}_c - \left[\frac{(\ddot{l}_1 + \ddot{l}_2 - \ddot{l}_3 - \ddot{l}_4)(l_1 + l_2 - l_3 - l_4)}{4(a - b - 23.75)\sqrt{16^2 - (l_3 + l_4 - l_1 - l_2)^2}} + \frac{(l_1 + l_2 - l_3 - l_4)^2(\dot{l}_1 + \dot{l}_2 - \dot{l}_3 - \dot{l}_4)^2}{4(a - b - 23.75\left[16c^2 - (l_3 + l_4 - l_1 - l_2)^2\right]^{\frac{3}{2}}} + \right.$$

$$\left.\frac{(l_1 + l_2 - l_3 - l_4)^2}{16c(a - b - 23.75)\sqrt{1 - \frac{l_1 + l_2 - l_3 - l_4}{4c}^2}}\right](z_c + 104) \tag{44}$$

$$\ddot{\theta} = \left[\frac{(\ddot{l}_1 + \ddot{l}_2 - \ddot{l}_3 - \ddot{l}_4)}{\sqrt{16c^2 - (l_3 + l_4 - l_1 - l_2)^2}}\right] - \left[\frac{(l_3 + l_4 - l_1 - l_2)(\dot{l}_1 + \dot{l}_2 - \dot{l}_3 - \dot{l}_4)^2}{(16c^2 - (l_3 + l_4 - l_1 - l_2)^2)^{\frac{3}{2}}}\right] \tag{45}$$

For the platform component, in order to find the applied force at each joint on the right hand side of equation (29a), first, the velocity components in equations (33), (39), (40), and (41) are substituted in equation (30). Then, obtain the derivative of equation (30) with respect to $\dot{l}_1$. So, this yields the first term of the left hand side of equation (29a). And the second and third term can be found by obtaining the derivative with respect to l_i of equations (30) and (31). So, the translational forces for each translational joint can be obtained, owing to mass and inertia of the platform component. The same procedures can be performed on the remaining components as shown in the equations (29b), (29c), (29d) and (29e). Finally, the total force (F_i) of the system

can be obtained by summing of all the resultant forces which are generated from masses and moments of inertia of other components.

5. Simulation and Results

The inverse kinematics and dynamic model obtained from previous section are implemented in MATLAB in order to compare the numerical solutions with the commercial dynamics software using the ADAMS solver.

Substitute all model constants or parameters used in the simulation such as $T_L = 163$ mm, $c = 37.5$ mm, $R = 587$ mm, $b = 57.25$ mm, $a = 215$ mm, $h = 1024.5$ mm, $p = 720$ mm, $d = 37.5$ mm and $Ec = 22.93$ mm. Properties of materials as mild steel are applied for the model components. So,

mass properties and moments of inertia can be found as follows:

$$m_{MH} = 14.0881 \; kg \quad \bar{I}_{MHy} = 994625.076 \; kgmm^2$$

$$m_{CH} = 9.36853 \; kg \quad \bar{I}_{XX,Am} = 105660 \; kgmm^2$$

$$m_{Am} = 2.71940 \; kg \quad \bar{I}_{YY,Am} = 105415 \; kgmm^2$$

$$m_{LJ} = 4.65962 \; kg \quad \bar{I}_{UCy} = 60.3645 \; kgmm^2$$

$$m_{UC} = 0.28739 \; kg$$
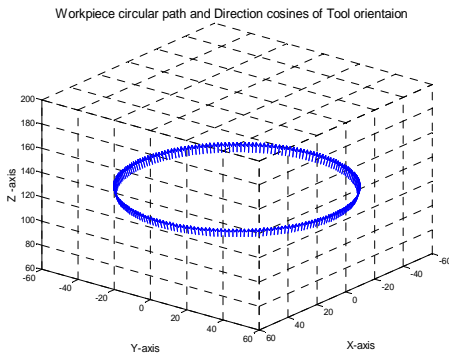
Figure 9 Orientation for path on spherical workpiece
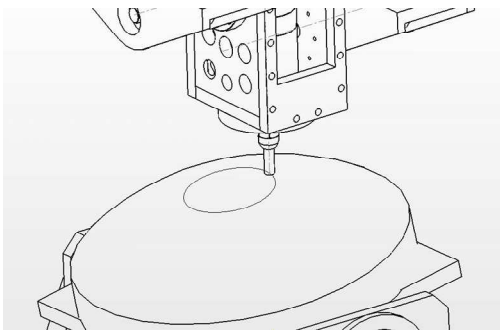
Figure 10 Circular path on spherical workpiece

Figure 9 shows the circular path on a spherical surface of a workpiece. The path is used for the evaluation of the inverse kinematics and the dynamic model. The diameter of this path is 104. 1889 mm.

During simulation, the tool-tip moves two times on the path and is always pointed toward to the direction normal to the plane which is tangent to the spherical surface along the circular path. The workpiece locations (x_w, y_w, z_w) and orientations of direction cosines (I_w, J_w, Z_w) from the desired trajectory path, defined in the working coordinate system, are used as reference inputs. So, the joint variables (l_1, l_2, l_3, l_4) of the system can be calculated from the derived inverse kinematics equations (5) to (10). The joint variables (l_1, l_2, l_3, l_4) obtained from the derived inverse kinematics are compared with the output results from the simulation using commercial packages based on ADAMS solver. The comparison results are illustrated in Figure 11 to Figure 14. The joint variables (α, θ) which were calculated from equations (9) and (10) are compared with results from simulation shown in Figures 13 to 14. Both angular errors are within 0.0128 degrees. The deviations in distances of linear joints between both results are within 0.12 mm. These errors are the result of accumulating angular error due to the usage of angular joint variables, which were calculated from the direction cosines as in equation (9) and (10).

Knowing the position and orientation of points on the circular path as shown in Figures 9 and 10, the variables q = $[l_1 \; l_2 \; l_3 \; l_4 \; \alpha \;]^T$ together with θ (rotating table) can be solved by inverse kinematics equations. The feed rate along the path is equal to 27.25 mm/sec or 1635.45 mm/min. The translation forces on each joint, four translational joints attached to both rails of the H-4 mechanism, can be obtained by substituting joint variables into the derived dynamic equation as detailed in the previous section. The joint variables consist of joint position, joint velocity, derived from inverse Jacobian in equation (25), and joint acceleration. The tool-tip location, along the desired path on the spherical surface, can be obtained from the derived equations as well as from the ADAMS solver. The GSTIFF algorithm of the ADAMS solver is used to obtain

numerical solution from the solid modeling of the manipulator arm with 24 seconds simulation time and 0.06 second for time increment. The comparison of the four translational forces obtained from the derived dynamic model and the commercial software for dynamics simulations are shown in Figure 15. The directions of all translational force are shown in Figure 8. Both figures illustrate that the resultant forces F2 and F4 are in opposite direction, with F1 and F4 and all of the forces trying to lift the platform up within the working area of the rotating table during tracking of the desired circular path. All of the resultant forces from the derived equations are very closed to all of the resultant forces obtained from the simulation model as shown in Figure 15. The differences of those forces for each joint are illustrated in Figure 16. The differences are within 0.0006 Newton. This implies that the derived dynamic model is accurate enough for using in the feedback control algorithm
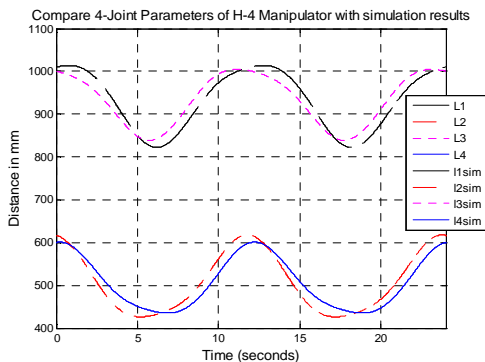
Figure 11 Distances of Translational joints *l1-l4* from inverse kinematics equation due to circular path
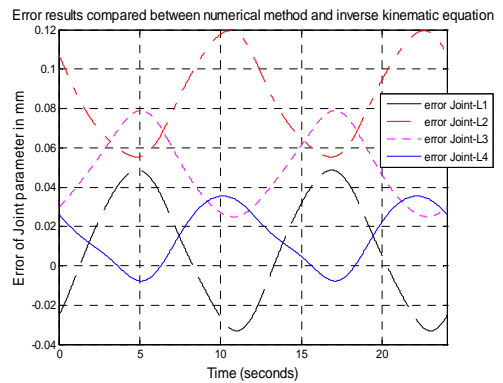
Figure 12 Error in Distances of Translational joints *l1-l4* between numerical method and derived inverse kinematics
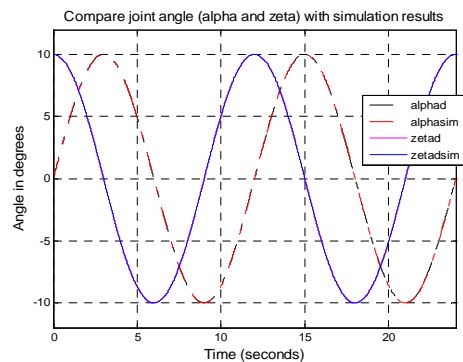

Figure 13 Platform rotation (θ) and turning table angle(α) compared between numerical method and derived inverse kinematics
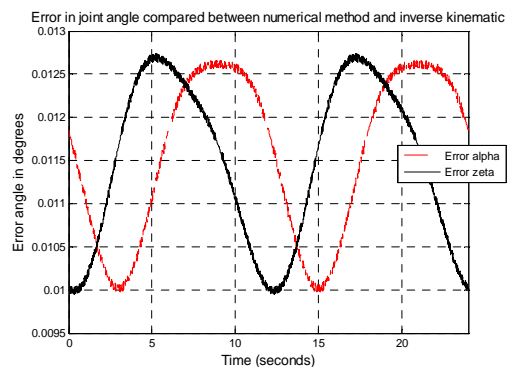

Figure 14 Error in Platform rotation (θ) and turning table angle (α) compared between numerical method and derived inverse kinematics
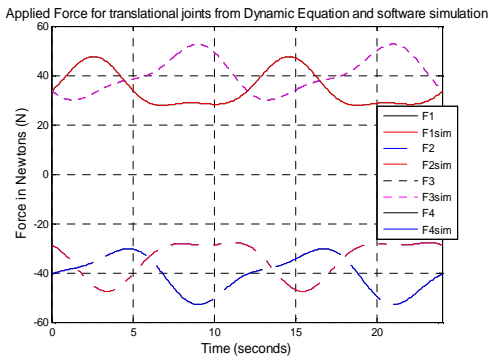
57

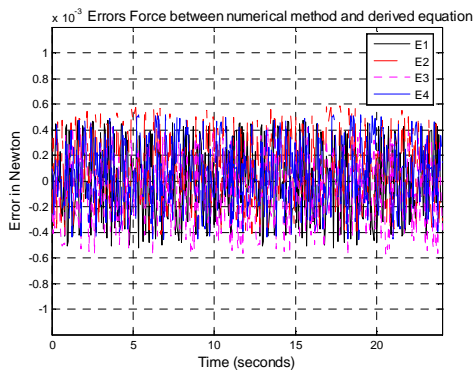**Figure 15** Translational Generating Force of joint *l1-l4*

Figure 16 Errors in Translational Force (N) of l_1, l_2, l_3, l_4 between numerical solutions of the analytical equation and the results from ADAMS.

6. Friction model from Experimental Results

According to dynamic equations derived in the previous section, an experiment has been set up to compare the joint torques from the derived model (inverse dynamic) with the measured joint torques. Inverse kinematics is used for obtaining the joint commands from the desired circular working paths as shown in Figure 10. The real mechanism using in this experiment has components constructed with the same sizes, and used the same materials as the model shown in Figure 7. The difference between this model and the real manipulator arm is the sets of motors and ball screws, which have

to be attached to the four linear components, on each rail. These must be calculated further after deriving force from the dynamic model equation as expressed in equation (29). Because of the real world, friction cannot be avoided in the real mechanism. The compensation model of friction has to be added up to the derived dynamic model.

The inputs to the control joint command system using inverse kinematics are the desired trajectories, described as a function of time as $x_T^{TP}(t) = \begin{bmatrix} x_w(t) & y_w(t) \\ z_w(t) & \theta(t) & \alpha(t) \end{bmatrix}^T$. The outputs are the joint torques to be applied at each instant by the brushless DC servo motors in order to follow the desired circular trajectories path. The output joint torques of four motors can be shown as solid line on Figure 17.

The desired actuated torque can be obtained by evaluating the right-hand side terms of the dynamic equations in (46) which get four translational forces as in Figure 15 :

$$F_i = \frac{d}{dt}\frac{\partial(K.E.)}{\partial \dot{l}_i} - \frac{\partial(K.E.)}{\partial l_i} + \frac{\partial(P.E.)}{\partial l_i} \quad i=1,2,3,4 \quad (46)$$

and

$$T_i = \frac{F_i D_p}{2}\left[\frac{L_d + \mu\pi D_p}{\pi D_p - \mu L_d}\right] + (J_{motor} + J_{screw})\left[\frac{2\pi\ddot{l}_i}{L_d}\right] + T_{friction1}$$
(47)

The torque in equation (47) is derived from the assumption that the platform is moving upward. The ball screws used have self-locking characteristics. So, the force needs to overcome the gravitational force distributes in the direction of the rail. For the opposite direction, the torque required to move the platform is:

$$T_i = \frac{F_i D_p}{2}\left[\frac{\mu\pi D_p - L_d}{\pi D_p + \mu L_d}\right] + (J_{motor} + J_{screw})\left[\frac{2\pi\ddot{l}_i}{L_d}\right] + T_{friction2}$$
(48)

D_p = pitch diameter of ball screw = 0.016 m

L_d = lead of the screw in mm per revolution = 0.005 m

μ = coefficient of friction for rolling contact as in [12]

 = 0.01687

$J_{motor}+J_{screw}$ = Inertia of rotor and Ball screw

 = 0.0000756877 kg-m^2 for motor 1,2,3

 = 0.0001576877 kg-m^2 for motor 4

$\tau_{friction}$ = overall resistant torque due to coulomb friction of all joints

The friction torques can be obtained by measuring the force or torque to move the rail on the ball screw. The friction torques are not constant, they are functions of angle θ. The linear regression model of the friction torque can be constructed as:

For motor1:

$$\tau_{friction1} = 0.0019743 * \theta + 0.205887 \qquad (49)$$

$$\tau_{friction2} = 0.0022429 * \theta + 0.087949 \qquad (50)$$

For motor2:

$$\tau_{friction1} = -0.00112815 * \theta + 0.25935 \qquad (51)$$

$$\tau_{friction2} = -0.00338445 * \theta + 0.13166 \qquad (52)$$

For motor3:

$$\tau_{friction1} = -0.0022563 * \theta + 0.179193 \qquad (53)$$

$$\tau_{friction2} = 0.00112815 * \theta + 0.0676595 \qquad (54)$$

For motor 4:

$$\tau_{friction1} = -0.000112815 * \theta + 0.4174155 \quad (55)$$

$$\tau_{friction2} = 0.00112815 * \theta + 0.2446005 \qquad (56)$$

while the angle θ is the rotation of the tool in units of degrees.

The torques evaluating from the equations (46)–(48) can be compared with the actuated torques measured from the experiment. The results of the comparison are shown in Figure 17. The average torques of each motor, which are shown as solid-line from the measurement, are close to the torques obtained from the derived dynamic model, which are shown as dashed line.
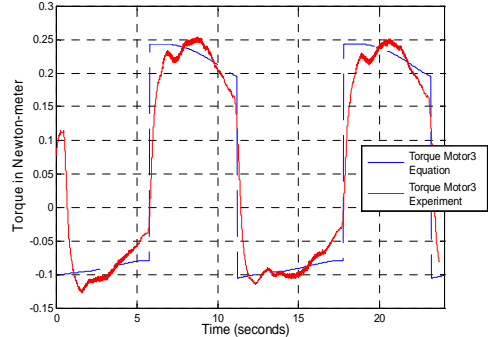

Torque of Actuator 1 compared between derived dynamics Equation and Experiment
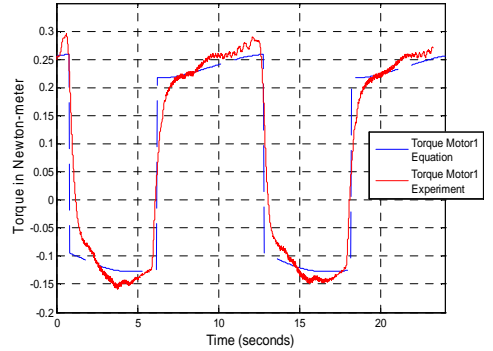
Torque of Actuator 2 compared between derived dynamics Equation and Experiment
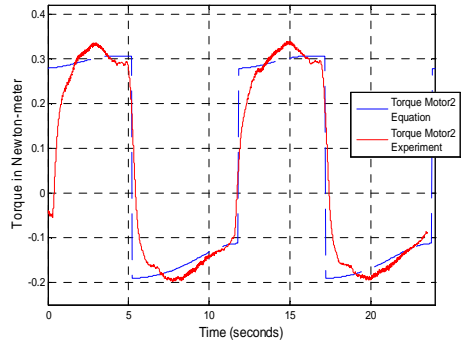
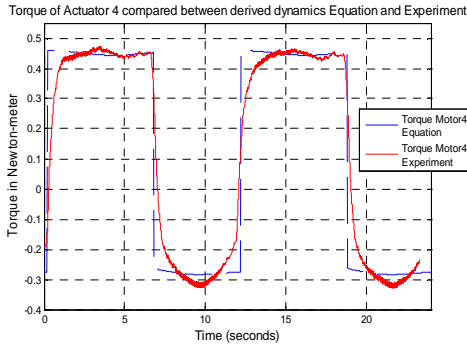Torque of Actuator 3 compared between derived dynamics Equation and Experiment

Figure 17 Compare torques between simulation model by derived equation and experi-ment.

7. Inverse Dynamics Control

In this section, the problem of tracking control of an operational space trajectory or a Cartesian space trajectory has been focused on as a testing experiment. The circular path on a spherical surface of a workpiece, as mention earlier, is used as the referenced path. The dynamic model of the manipulator arm can be written in the well known format as shown in equation (57). It is nonlinear and multivariable system described as:

$$B(q)\ddot{q} + C(q,\dot{q})\dot{q} + F\dot{q} + g(q) = \tau \quad (57)$$

The resolved acceleration control is implemented based on the derived dynamic model. It is a feedback linearization control technique for tracking control problem. The controlled torques can be derived from the inverse dynamic model as in equation (58). The inverse dynamic model can be obtained from the derived dynamic model as in the equations (46)–(48) as:

$$\tau = B(q)v + C(q,\dot{q})\dot{q} + F\dot{q} + g(q) \quad (58)$$

Substitute torques from equation (58) into equation (57), and the linear model used for controller design can be described by:

$$\ddot{q} = v \quad (59)$$

where v can be considered as the resolved acceleration in terms of joint space whose expression is to be determined yet. From the analytical Jacobian in equation (25), the velocity relationship between end-effector and joint manipulator is written in the form:

$$v_e = J_A^{-1}(q)\dot{q} \quad (60)$$

The acceleration, $a = \dot{v}_e = \ddot{x}_e$, can be derived from equation (60). The resolved acceleration can be chosen as:

$$v = J(q)\left[a - \dot{J}^{-1}(q,\dot{q})\dot{q}\right] \quad (61)$$

where $a = \dot{v}_e = \ddot{x}_e$ (62)

a can be considered as the resolved acceleration in terms of end-effector variables and can be selected as:

$$a = \ddot{x}_d + K_D(\dot{x}_d - \dot{x}_e) + K_p(x_d - x_e) \quad (63)$$

where $x_d, \dot{x}_d, \ddot{x}_d$ is the desired path trajectory, end-effector velocity, and end-effector acceleration. So, equation (63) can be turned into a homogeneous differential equation as:

$$\ddot{\tilde{x}} + K_D\dot{\tilde{x}} + K_p\tilde{x} = 0 \quad (64)$$

where $\tilde{x} = x_d - x$. Equation (64) expresses the dynamics of position error, $\tilde{x}$, while tracking the given trajectory, $x_d, \dot{x}_d, \ddot{x}_d$. The gain K_p, K_D can be selected by specifying the desired feedrate.

The block diagram of the control system is illustrated in Figure 18. The

trajectory, $x_d, \dot{x}_d, \ddot{x}_d$, can be defined based on the specified circular path on a spherical surface. $\alpha_d, \dot{\alpha}_d$ are the desired angular position and velocity, respectively, of the rotating table. So, the referenced input can be written as $x_d(t) = [x_{ud}(t) \ y_{ud}$ $(t) \ z_{ud}(t) \ \theta_d(t) \ \alpha_d(t)]^T$ and $\dot{x}_d, \ddot{x}_d$. The command torques can be derived from the inverse dynamic model as in equations (46) – (48). And the end-effector position and velocity in operational space can be derived from the forward kinematics in (7a)-(7c) and inverse matrices of Jacobian in (25) as derived earlier.
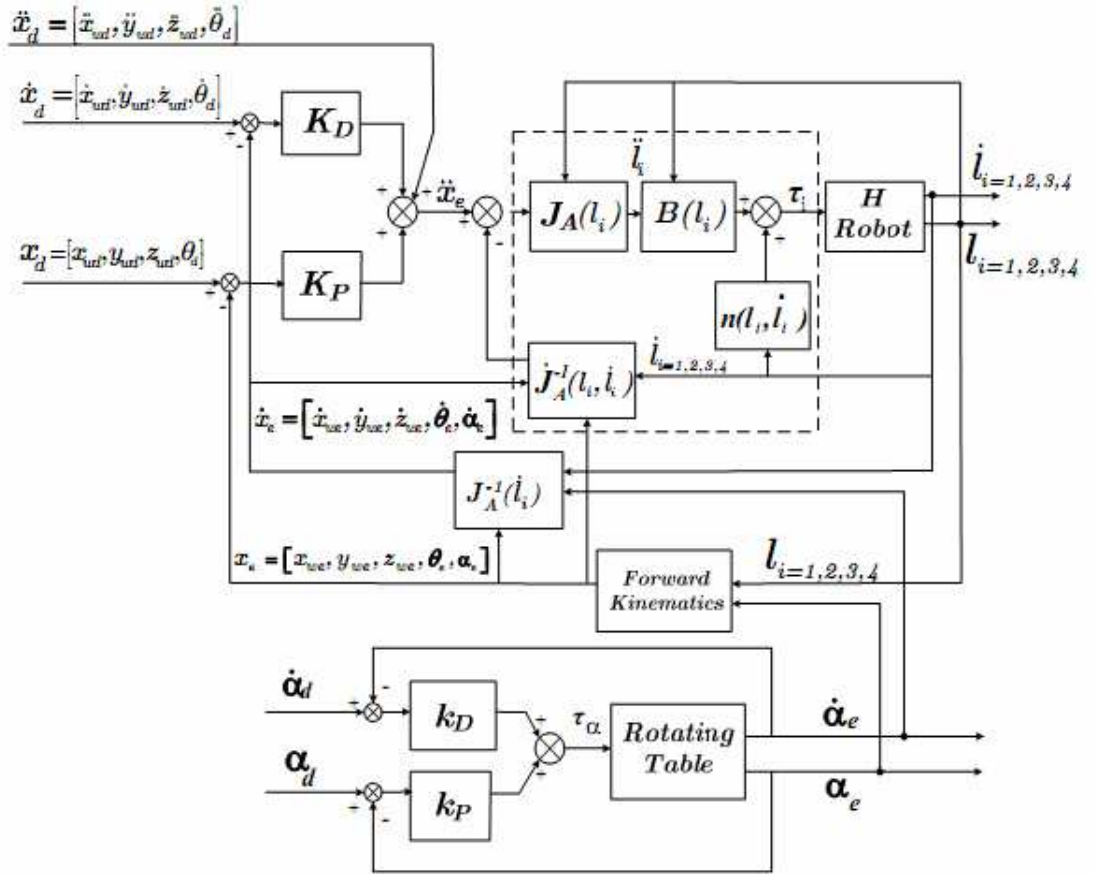

Figure 18 Block scheme of operational space inverse dynamics control

The position and velocity gain used in equation (64) is chosen as:

$$K_p \begin{bmatrix} 8400 & 0 & 0 & 0 \\ 0 & 8000 & 0 & 0 \\ 0 & 0 & 8000 & 0 \\ 0 & 0 & 0 & 7000 \end{bmatrix}$$

$$K_D \begin{bmatrix} 90 & 0 & 0 & 0 \\ 0 & 80 & 0 & 0 \\ 0 & 0 & 80 & 0 \\ 0 & 0 & 0 & 80 \end{bmatrix}$$

Whereas the PD gains of the rotating table are:

$$K_p = 550.0 \qquad K_D = 4.0$$

The resistant torque models due to coulomb friction are also used in the control system as feed forward for compensation of the actual friction torques in the system. From equations (49)-(56), friction torques obtained earlier need to be modified (offset part) so that good responses are achieved. The modified friction torques are as follows:

For motor1:
$$\tau_{friction1} = 0.0019743 * \theta + 0.15$$
$$\tau_{friction2} = 0.0022429 * \theta + 0.1$$

For motor2:
$$\tau_{friction1} = -0.00112815 * \theta + 0.15$$
$$\tau_{friction2} = -0.00338445 * \theta + 0.1$$

For motor3:
$$\tau_{friction1} = -0.0022563 * \theta + 0.15$$
$$\tau_{friction2} = 0.00112815 * \theta + 0.1$$

For motor 4:
$$\tau_{friction1} = -0.000112815 * \theta + 0.3$$
$$\tau_{friction2} = 0.00112815 * \theta + 0.2$$

In the experiment, the tool-tip is desired to maintain the direction normal to the plane, tangent to the spherical surface, at the point of contact along the desired path. The tool-tip moves twice on the circular path. The feed rate is set equal to 27.3273 mm/sec or 1639.638 mm/min.

The experimental results are shown in Figure 19 – Figure 26. Figure 19 shows the measurement of the tool-tip position (x_{we}, y_{we}, z_{we}) in the workpiece X_W-Y_W-Z_W coordinate compared with the desired reference (x_{wd}, y_{wd}, z_{wd}). The desired z_{wd} references in Z_W coordinate is maintained at a constant level at 116 mm. The actual tool-tip position is close to the reference position. The desired motion of x_{wd} and y_{wd} in X_W and Y_W direction are sinusoidal motion. The error between the measured tool-tip position and desired reference position of each axis can be found as x_{we}-x_{wd}, y_{we}-y_{wd} and z_{we}-z_{wd} and set as XwError, YwError and ZwError, respectively, which are shown in Figure 20 - Figure 22. By observing those figures, it can be found that the maximum errors occur in the X_W coordinate which is in the same direction of the translational joints, and maximum sizes of error occur when the direction of the four linear translational joints motion are changed. All Errors in X_W Y_W and Z_W directions have similar patterns. At the start point and the end point of motion, there are also more illustrations of error. These errors can be reduced by adding dither signal, embedded in the command signal, to prevent the motion getting struck because of friction. The maximum error, after friction compensation, occurs in the X_W direction and is less than 0.35 mm. Figure 23 illustrates the measurement of tool rotation (θ_e) and turning table angle (α_e). The desired angular motions at tool-center (θ_d) and table (α_d), in Y and Z directions, are defined as sinusoidal motion which is 10 degrees in amplitude and 90 degrees difference in phase angle. The actual tool and table angles are close to the desired referenced angle. The difference in measured angles from the desired can be illustrated as Zeta Error or θ_e-θ_d and Alpha Error or $\alpha_e - \alpha_d$ as shown in Figure 24 and Figure 25. The maximum angular errors at tool rotation and at the rotating table are less than 0.12 degree for θ and 0.15 degree for α, respectively. Figure 26 shows feed speed which is calculated from the actual tool-tip velocity $(\dot{x}_{we}, \dot{y}_{we}, \dot{z}_{we})$ in the workpiece coordinates, X_W-Y_W-Z_W, compared with the tool-tip desired feed velocity which is calculated from the

desired reference velocity ($\dot{x}_{wd}$, $\dot{y}_{wd}$, $\dot{z}_{wd}$).

The actual feed speed is a little bit higher than the desired feed and has some small jerks which have much high velocity error. These velocity jerks occur during the motion of each joint, changing direction and friction cause motion to get struck for small time intervals, and start moving again with discontinuous velocity. If more accurate control is needed, the dither signal has to more carefully adjusted. The desired feed speed, 27.3273 mm/sec, used in this experiment is rather larger than typical cutting speed for conventional machine tools. Small backlash and structure flexibility also create sources of error. Because, in the experiment, the tool-tip position is calculated from the kinematic formulation, the numerical truncation error also creates another source of error.
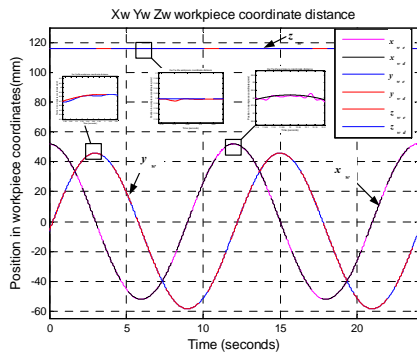

Figure 19 Tool-Tip position in workpiece coordinates Xw,Yw,Zw measurement on circular path
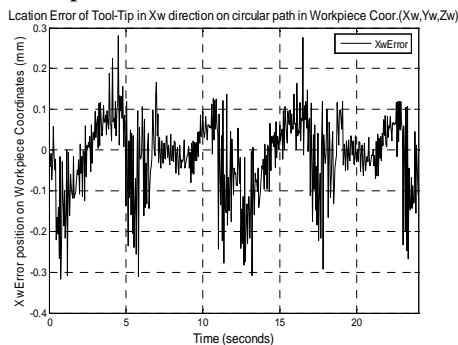

Figure 20 Xw Tool-Tip position error in workpiece coordinates Xw, Yw, Zw com-

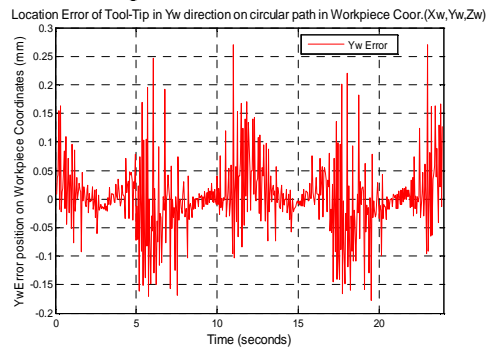pared between actual path measurement and desired path

Figure 21 Yw Tool-Tip position error in workpiece coordinates Xw, Yw, Zw compared between actual path measurement and desired path
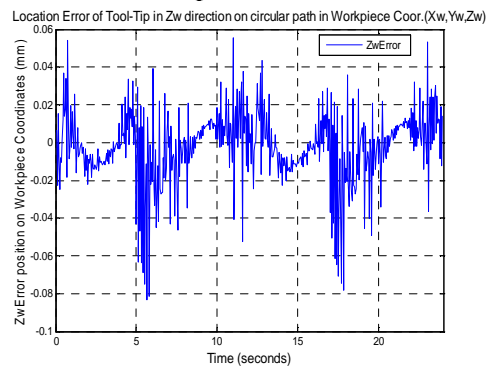

Figure 22 Zw Tool-Tip position error in workpiece coordinates Xw, Yw, Zw compared between actual path measurement and desired path
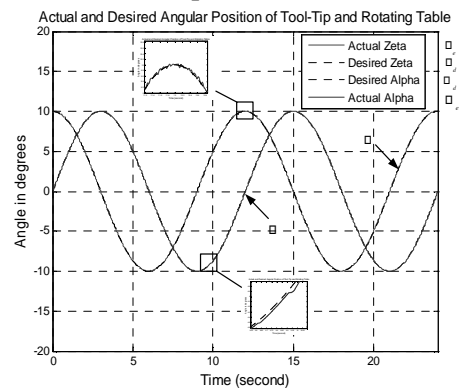

Figure 23 Tool rotation angle (θ) and turning table angle(α) measurement on circular path
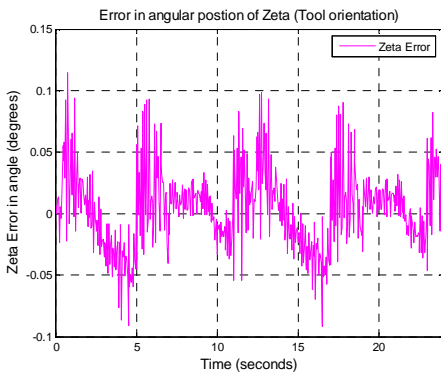
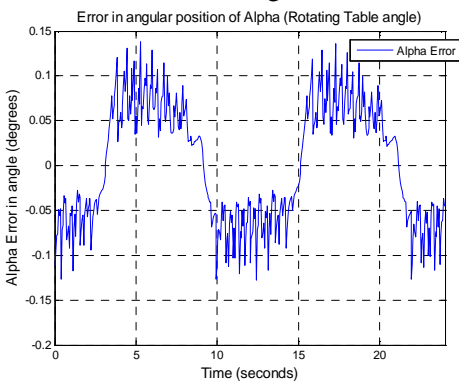**Figure 24** Error of the tool rotation angel (θ) between the actual angular measurement and the desired angle

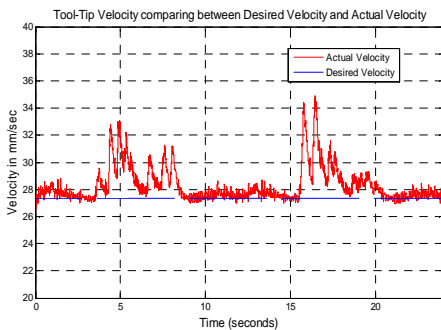**Figure 25** Error of the turning table angular (α) between the actual angular measurement and the desired angle

Figure 26 Tool-Tip velocity in workpiece coordinates Xw, Yw, Zw

8. Conclusion

This paper presented the kinematics analysis, Jacobian and the Dynamic Model of the 5-DOF parallel mechanism design based on H-4 family with addition of a single axis rotating table. The dynamic equations are derived from the Lagrangian formulation. The numerical results of the analysis of kinematics, Jacobian and the dynamic model are compared with numerical results from a popular commercial software, the ADAMS solver, using the virtual model data. This is to assure the accuracy of the derived model and the possibility of using it in the feedback system. Friction models obtained from the experiment are used to compensate for the actual friction of the system in the resolve acceleration control strategy. Inverse dynamics is implemented in the first four axis of the H-4 parallel manipulator to perform feedback linearization. The circular trajectory on a spherical surface is used as the reference profile for tracking control. The tracking performance can be improved by increasing the rigidity of the structure and reducing the numerical truncation error.

The kinematic equations, Jacobian, and dynamic model obtained in this paper are suitable for implementing in real time control. The manipulator is used for cutting complex surface of soft materials. The purposed manipulator (slave arm) with the 6-DOF haptic device (master arm) developed in-house [15] can be used in tele-operation with force reflection. Force control algorithms are implemented to help an operator to gain better feeling of maneuvering the master arm during the slave arm cutting a surface as shown in Figure 27. In this paper, we concentrated on only the slave arm. The complete operation of the tele-operation with force reflection will be presented in the future.

The master arm with force reflection   The Slave arm (5-axis)

Figure 27 Master-Slave Arm Haptic device

9. References

[1] Monsarrat, B. and Gosselin, C. M., Singularity Analysis of a Three-Leg 6Dof parallel Grassmann Line Geometry, International Journal of Robotics Research, Vol.20, No.4, April 2001, pp. 312-326.

[2] Tsai, L. W., Robot Analysis-The Mechanics of Serial and Parallel Manipulators, John Wiley & Sons, 1999.

[3] Clavel, R., Conception d'un Robot Parallèle Rapide à 4 degrés de liberté, Ph.D. Thesis, EPFL, Lausanne, Switzerland, 1991.

[4] Pierrot, F., H4_a New Family of 4-DOF Parallel Robots, IEEE/ASME Advanced Intelligent Mechatronics Conf. Proc. Atlanta USA, September 1999, pp. 508-513.

[5] Park, K.W. and Lee M.K., Workspace and Singularity Analysis of a Double Parallel Manipulator IEEE/ASME Transactions on Mechatronics, Vol. 5, No. 4, December 2000, pp. 367-375.

[6] Chiu, Y.J. and Perng, M.H., Forward Kinematics of a General Fully Parallel Manipulator with Auxiliary Sensors. International Journal of Robotics Research, Vol.20, No.5, May 2001, pp. 401-414.

[7] Pierrot, F.and Marquet, F., H4 Parallel Robot Modeling Design and Preliminary Experiments, IEEE Robotics and Automation Conf. Proc., Seoul Korea, May 2001, pp. 3256-3261.

[8] Viboon S. and Natdanai T., Design of the new 4-DOF Parallel Manipulator with Object Contact Force Control, The 19th Conference of Mechanical Engineering Network of Thailand, October 2005.

[9] E.L.J. Bohez , Computer Control of Manufacturing I., Asian Institiute of Technology, Bangkok, Thailand, December 1995.

[10] E.L.J. Bohez, Compensating for Systematic Errors in 5-axis NC Machining., Computer-Aided Design, 30 March 2001.

[11] Chung-Ching Lee, Jeng-Hong Chiu and Hung-Hui Wu , Kinematics of a H- Type Pure Translational Parallel Manipulator, Proceeding of IDETC/CIE 2005 ASME 2005, International Design Engineering Technical Conf., September 24-28,2005.

[12] Dumitru Olaru, George C. Puiu, Liviu C. and Balan, Vasile Puiu, A New Model to Estimate Friction Torque in a Ball Screw System, Product Engineering Springer, Netherlands, pp.333-346,2005

[13] Sangveraphunsiri,V. and Tantawiroon N., Novel Design of a 4 DOF Parallel Robot., 2003 JSAE Annual Congress, Yokohama, Japan, May 21-23, 2003.

[14] Sangveraphunsiri,V. and Tantawiroon N., Design and Analysis of a New H-4 Family Parallel Manipulator, Thammasat International Journal of Science and Technology, Vol.10, No.3, July-September, 2005, pp. 38-52.

[15] Viboon Sangveraphunsiri and Tawee Ngamvilaikorn, Design and Analysis of 6 DOF Haptic Device for Teleoperation Using a Singularity-Free Parellel Mechanism, Thammasat International Journal of Science and Technology, Vol.10, No.4, October-December, 2005, pp. 60-69.

[16] Viboon Sangveraphunsiri and Prasartporn Wongkumchang, Design and Control of a Stewart Platform, the 15th National Conference of Mechanical Engineering, 2001, (in Thai).

[17] W. Anotaipaiboon, SS. Makhanov and E.L.J. Bohez , Optimal Setup for 5-axis Machining., International Journal of Machine Tools & Manufacture, 28 July 2005.

[18] Stewart, D., A Platform with 6 Degrees of Freedom., Proc., Institution of Mechanical Engineers, 180 (part 1, 15,pp.371-386),1965.

[19] Richard M. Murray, Zexiang Li and S. Shankar Sastry, A Mathematical Introduction to Robotic manipulation, CRC Press, Inc. 1993.